

4

DTIC FILE COPY

AD-A207 759

TECHNICAL REPORT BRL-TR-2998

BRL

COLLISIONAL TRANSFER BETWEEN AND QUENCHING
OF THE 3P ³P AND ⁵P STATES
OF THE OXYGEN ATOM

S DTIC
ELECTE
MAY 16 1989 **D**
D

BRAD E. FORCH
ANDRZEJ W. MIZIOLEK
PAUL J. DAGDIGIAN

MAY 1989

APPROVED FOR PUBLIC RELEASE; DISTRIBUTION UNLIMITED.

U.S. ARMY LABORATORY COMMAND

BALLISTIC RESEARCH LABORATORY
ABERDEEN PROVING GROUND, MARYLAND

89 5 15 055

UNCLASSIFIED

SECURITY CLASSIFICATION OF THIS PAGE

REPORT DOCUMENTATION PAGE				Form Approved OMB No. 0704-0188	
1a. REPORT SECURITY CLASSIFICATION Unclassified			1b. RESTRICTIVE MARKINGS		
2a. SECURITY CLASSIFICATION AUTHORITY			3. DISTRIBUTION / AVAILABILITY OF REPORT APPROVED FOR PUBLIC RELEASE; DISTRIBUTION UNLIMITED		
2b. DECLASSIFICATION / DOWNGRADING SCHEDULE					
4. PERFORMING ORGANIZATION REPORT NUMBER(S) BRL-TR-2998			5. MONITORING ORGANIZATION REPORT NUMBER(S)		
6a. NAME OF PERFORMING ORGANIZATION US Army Ballistic Research Laboratory		6b. OFFICE SYMBOL (If applicable) SLCRR-IB	7a. NAME OF MONITORING ORGANIZATION		
6c. ADDRESS (City, State, and ZIP Code) Aberdeen Proving Ground, MD 21005-5066			7b. ADDRESS (City, State, and ZIP Code)		
8a. NAME OF FUNDING / SPONSORING ORGANIZATION		8b. OFFICE SYMBOL (If applicable)	9. PROCUREMENT INSTRUMENT IDENTIFICATION NUMBER		
8c. ADDRESS (City, State, and ZIP Code)			10. SOURCE OF FUNDING NUMBERS		
		PROGRAM ELEMENT NO. 61102A	PROJECT NO. AH43	TASK NO.	WORK UNIT ACCESSION NO.
11. TITLE (Include Security Classification) COLLISIONAL TRANSFER BETWEEN AND QUENCHING OF THE $3p^3P$ AND $5p^5P$ STATES OF THE OXYGEN ATOM					
12. PERSONAL AUTHOR(S) Paul J. Dagdigian*, Brad E. Forch, Andrzej W. Miziolek					
13a. TYPE OF REPORT Final		13b. TIME COVERED FROM Oct 87 TO Sep 88		14. DATE OF REPORT (Year, Month, Day)	15. PAGE COUNT
16. SUPPLEMENTARY NOTATION *The Johns Hopkins University Published in Chemical Physics Letters					
17. COSATI CODES			18. SUBJECT TERMS (Continue on reverse if necessary and identify by block number)		
FIELD	GROUP	SUB-GROUP	Excitation Transfer, Oxygen Atoms, Quenching, Two-Photon Fluorescence, Nitrogen. (mgn)		
20	05				
21	02				
19. ABSTRACT (Continue on reverse if necessary and identify by block number) Collisional quenching and excitation transfer between the oxygen atom $3p^3P$ and $5p^5P$ states have been investigated in a discharge flow apparatus with O_2 and N_2 collisional partners. The $3P$ state was excited by two-photon excitation at 225.6 nm from the $2p^4^3P$ ground state, and temporal profiles of the $3P \rightarrow 3S$ and $5P \rightarrow 5S$ emission at 844.7 and 777.5 nm, respectively, to the lower 3s manifold were recorded. From an analysis of $3P$ decay curves as a function of quencher pressure, the following bimolecular rate constants for the removal of the $3P$ state were determined: $k_3^O(O_2) = (7.8 \pm 0.8) \times 10^{-10}$ and $k_3^O(N_2) = (5.87 \pm 0.15) \times 10^{-10}$ molecule $^{-1}$ cm 3 s $^{-1}$. The intercept of the O_2 Stern-Vollmer plot yielded $k_3^R = (2.98 \pm 0.15) \times 10^7$ s $^{-1}$ for the $3P$ radiative decay rate. The collisional quenching rate constant for the $5P$ state by O_2 was obtained by analysis of $5P$ decay curves: $k_5^O(O_2) = (10.8 \pm 1.8) \times 10^{-10}$ molecule $^{-1}$ cm 3 s $^{-1}$. Rate constants k_{35} for $3P \rightarrow 5P$ excitation transfer were obtained from measurements of the ratio of the $5P \rightarrow 5S$ to $3P \rightarrow 3S$ emission intensities as a function of					
20. DISTRIBUTION / AVAILABILITY OF ABSTRACT <input type="checkbox"/> UNCLASSIFIED/UNLIMITED <input checked="" type="checkbox"/> SAME AS RPT. <input type="checkbox"/> DTIC USERS			21. ABSTRACT SECURITY CLASSIFICATION Unclassified		
22a. NAME OF RESPONSIBLE INDIVIDUAL DR. ANDRZEJ W. MIZIOLEK			22b. TELEPHONE (Include Area Code) 301-278-6157	22c. OFFICE SYMBOL SLCRR-IB-I	

DD Form 1473, JUN 86

Previous editions are obsolete.

SECURITY CLASSIFICATION OF THIS PAGE

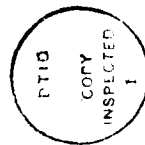
UNCLASSIFIED

19. Abstract (Cont'd):

quencher pressure. We find $k_{35}(\text{O}_2) \approx 6 \times 10^{-11}$ and $k_{35}(\text{N}_2) \approx 2 \times 10^{-11}$ molecule⁻¹ cm³ s⁻¹. These measurements are important for quantitative determination of oxygen atoms in combustion environments and for multiphoton photochemical ignition of reactive gases which involve oxygen-atom two-photon transitions at 225.6 nm.

TABLE OF CONTENTS

	<u>Page</u>
LIST OF FIGURES.....	5
I. INTRODUCTION.....	7
II. EXPERIMENTAL.....	9
III. RESULTS.....	10
A. Fluorescence Waveforms.....	10
B. Kinetic Equations.....	12
C. Quenching Rate Constants.....	13
D. Energy Transfer Rate Constants.....	15
IV. DISCUSSION.....	18
ACKNOWLEDGEMENT.....	21
REFERENCES.....	23
DISTRIBUTION LIST.....	25



Accession For	
NTIS CRA&I	<input checked="" type="checkbox"/>
DTIC TAB	<input type="checkbox"/>
Unannounced	<input type="checkbox"/>
Justification	
By	
Distribution/	
Availability Codes	
Dist	Avail and/or Special
A-1	

LIST OF FIGURES

<u>Figure</u>		<u>Page</u>
1	Relevant Energy Levels for Two-Photon Excitation of Oxygen Atoms and Excited-State Collisional Energy Transfer.....	8
2	Schematic Diagram of the Experimental Apparatus.....	9
3	Waveforms for (a) the $3P + 3S$ and (b) the $5P + 3S$ Fluorescence Emission Upon Two-Photon Excitation of the $3p\ 3P$ State.....	11
4	Stern-Volmer Plots for (a) the $3P + 3S$ Emission at 844.7 nm and (b) the $5P + 5S$ Emission at 777.5 nm as a Function of O_2 Quencher Partial Pressure.....	14
5	Ratio of the Integrated $5P + 5S$ to $3P + 3S$ Emission Intensity Versus added (a) O_2 and (b) N_2	16

I. INTRODUCTION

There is a considerable need for well-characterized diagnostic techniques for the quantitative measurement of the concentrations of species in propellant flames and other combustion environments. The use of multiphoton excitation schemes for the detection of light atoms, such as oxygen, has drawn considerable interest in recent years.¹⁻¹² Two different approaches have been employed in these methods, namely observation of the fluorescence emission from the multiphoton-excited resonant state¹⁻³ or absorption of an additional photon to produce ionization.⁸⁻¹² Both of these schemes have been utilized for the detection of hydrogen and oxygen atoms in flames. The former method has advantages over the latter in that it does not require the insertion of a probe into the medium and can also be used to obtain two-dimensional images of atomic concentrations in flames, as has recently been demonstrated.^{13,14} It is also easier to discriminate against background photon emission than ionization.

Figure 1 illustrates the scheme which has been used for the detection of oxygen atoms.^{1,3,5,6,8,13,14} Here, oxygen atoms are excited in a two-photon transition to the $3p\ ^3P$ state with 225.6 nm laser radiation and are detected by observation of the fluorescent emission to the $3s\ ^3S$ state at 844.7 nm. A number of parameters are required for the use of this diagnostic tool in a quantitative fashion. Recently, Bamford, et al.,⁸ have reported absolute cross sections for the two-photon absorption process, as well as for one-photon photoionization of the 3P state. Bimolecular collision quenching rate constants for this state have also been measured by several groups.^{1,6,8} These data are required to account for collisional effects in finite-pressure environments.

Miziolek and DeWilde⁵ have also shown the potential importance of collisional excitation transfer processes in the collisional removal of this highly excited atomic state. They excited oxygen atoms by two-photon absorption at 225.6 nm in an atmosphere-pressure $CH_4-N_2O-N_2$ flame and observed within and through the flame front not only $^3P \rightarrow ^3S$ emission at 844.7 nm, but also $^5P \rightarrow ^5S$ emission of even greater intensity at 777.5 nm. Similar detection of 777.5 nm emission was subsequently observed in imaging studies of atomic oxygen in flames.^{13,14} These observations suggest the occurrence of excitation transfer from the 3P to the 5P state (see Figure 1). The interpretation of these experiments in terms of specific bimolecular rate processes is not straightforward because of the high pressure (1 atmosphere) and chemical complexity of these flames. In addition, at least in the experiment of Miziolek and DeWilde,⁵ the tightly focused laser probe was observed to be promoting multiphoton photolysis of the oxidizer as well as the fuel molecules, leading to a two-photon resonant formation of a microplasma. Nevertheless, even under conditions of no apparent laser probe volume perturbation, it appears that spin-changing collisions of the initially excited level could be a significant collisional removal pathway for laser excited oxygen $3p\ ^3P$ atoms. In order to employ two-photon excitation for quantitative measurements in combustion environments, such as propellant flames, it is necessary to understand the mechanism for transfer of the initial excitation energy.

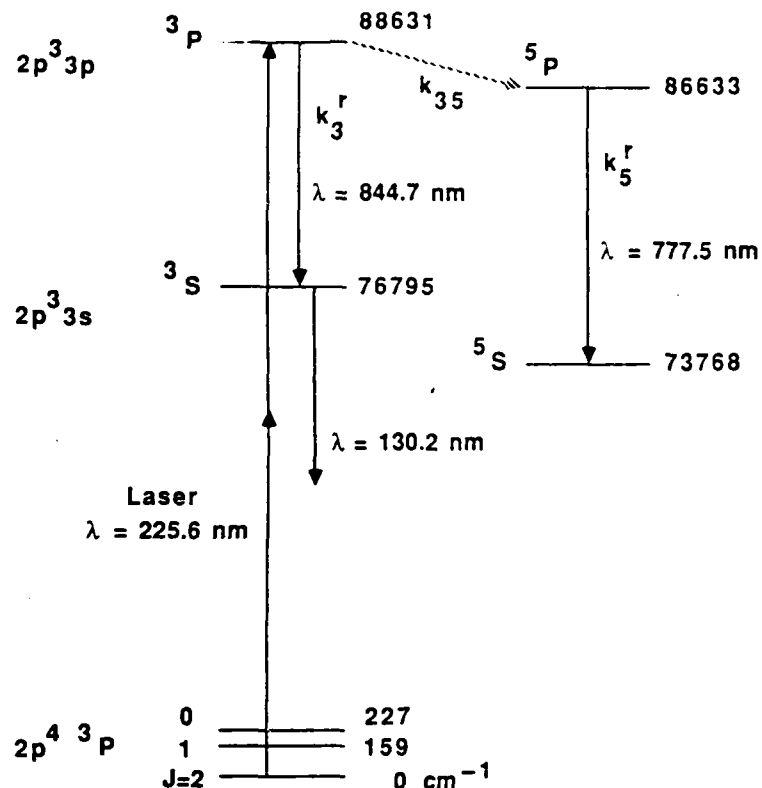


Figure 1. Relevant Energy Levels for Two-Photon Excitation of Oxygen Atoms and Excited-State Collisional Energy Transfer. The electronic energies, taken from Ref. 16 are given in cm^{-1} , and allowed radiative transitions are denoted, with wavelengths given in nm. The denoted radiative and collisional rate constants are defined in Section B.

The present experimental study was undertaken to investigate collisional excitation transfer from the oxygen $3p^3 3p$ to $5p$ states in a controlled low-pressure environment. Previous studies^{1,6,8} of collisional processes involving the $3p$ state have centered on the measurement of total quenching rate constants with closed-shell collisional partners, such as the inert gases, nitrogen molecules, etc. Simple theoretical considerations¹⁶ suggest that open-shell free radical species will be more effective in inducing spin-changing excitation transfer to the $5p$ state. Approach of an open-shell perturber species in a state of, say, doublet spin multiplicity to an oxygen atom in the $3p^3 3p$ state will yield both doublet and quartet molecular curves, while approach to the $5p$ state yields quartet and sextet states. Crossing of quartet curves originating from the $3p$ and $5p$ asymptotes will provide a spin-allowed mechanism for collision-induced transitions between the $3p$ and $5p$ states, which is not possible with closed-shell partners. This argument ignores the possible importance of excitations in the collision partner.

In the present study, we compare the propensity of the stable open-shell oxygen molecule and the closed-shell nitrogen molecule to induce $3p \rightarrow 5p$

transitions. Previous experiments^{1,6,8} have determined the total bimolecular quenching rate constants for quenching of the 3P state by these molecules.

II. EXPERIMENTAL

The apparatus employed for these experiments is shown in Figure 2. Oxygen atoms were generated by passing a mixture of helium and oxygen (typical partial pressures of 1.2 and 0.2 Torr, respectively) through an Evenson-Broida 2450 MHz resonant cavity. UHP grade gases were obtained from Linde and used without further purification. The walls of discharge tube were coated with phosphoric acid to reduce atomic recombination on the surfaces.¹⁷ The forward microwave power was kept relatively low (<25 W) in order to minimize the fractional dissociation of the oxygen molecules and production of other transient species. Nevertheless, this production scheme prepared sufficient densities of ground-state oxygen atoms for these experiments. The quenching gases, either N_2 or additional O_2 , were added downstream of the microwave discharge. Pressures were measured by a capacitance manometer. The flow tube was pumped by a 50 cfm single-stage mechanical pump.

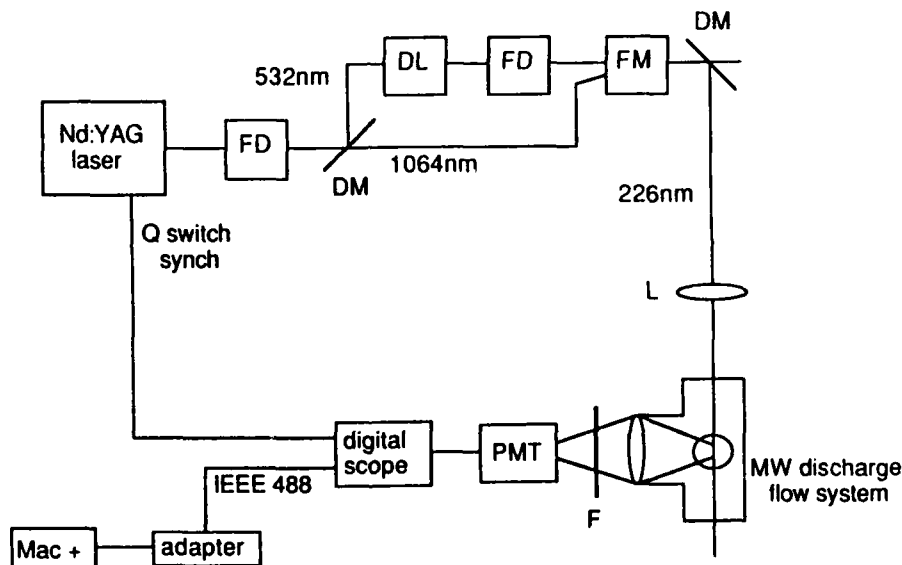


Figure 2. Schematic Diagram of the Experimental Apparatus.
DL: dye laser; FD: frequency-doubling crystal; FM: frequency-mixing crystal; DM: dichroic mirror; L: lens; F: interference filter; PMT: photomultiplier tube.

The laser excitation and fluorescence detection zone was located 10 cm beyond a 90° bend Wood's horn light trap, which itself was placed just past the microwave discharge. Two-photon excitation of oxygen atoms was accomplished with tunable uv radiation from a Nd:YAG pumped, frequency doubled and mixed dye laser (Quantel) which operated at a 10 Hz repetition rate. The dye solution in the latter was a concentration- and composition-tuned mixture

of rhodamine 590 and 610. The 226 nm radiation was separated from other wavelengths by a dichroic mirror; this separation technique was preferred over the use of prisms since, with the former, the laser beam position through the flow system does not change with wavelength. Typical uv power at the apparatus was approximately 1 mJ per pulse, and the bandwidth of the doubled and mixed radiation was ca. 1 cm^{-1} FWHM. The radiation was focused into the center of a flow system with a 30 cm Suprasil lens. No photolytic effects due to laser decomposition of molecular oxygen were evident, as observation of the O atom two-photon signal required the presence of both molecular oxygen and microwave radiation.

The fluorescence was collected at right angles to the laser beam with a fast (f/2) Suprasil lens and focused through a filter onto a red-sensitive photomultiplier tube (EMI 9516QB). The filters employed were a 850 nm center wavelength, 25 nm bandpass interference filter for detection of the $^3\text{P} \rightarrow ^3\text{S}$ emission at 844.7 nm and a 780 nm center wavelength, 10 nm bandpass filter for observation of the $^5\text{P} \rightarrow ^5\text{S}$ at 777.5 nm. The measured transmission of these filters was 56 and 66% at 844.7 and 777.5 nm, respectively.

The output from the photomultiplier was passed to a boxcar integrator (Stanford Research Systems) for measuring excitation spectra or to a digital oscilloscope (Tektronix 2430A) for capturing the temporal profiles of fluorescence waveforms. The boxcar integrator and oscilloscope were triggered with a synchronization pulse from the Nd:YAG laser Q switch. Some details about the specifications of the oscilloscope are relevant. The bandwidth of the analog section of this instrument is 125 MHz; the digital sampling rate is 100 megasamples per sec, or 10 nsec between channels. In our experiments we utilized an interpolation feature for repetitive signals, which allowed digitization on a finer grid to achieve the full bandwidth: The waveform from an individual laser pulse was obtained with the usual 10 nsec spacing; however, successive waveforms were taken with a slightly shifted initial delay, controlled internally by the oscilloscope. To improve the signal-to-noise ratio, waveforms were also acquired using a 256-scan running average. Typical emission lifetimes ranged from 40 to 15 nsec, while the laser excitation pulse length was 7 nsec.

The waveforms acquired by the digital oscilloscope were transferred through an IEEE 488 interface to a microcomputer (Apple Macintosh Plus) for storage, generation of hard-copy plots, and analysis.

III. RESULTS

A. Fluorescence Waveforms:

Figure 3 displays typical fluorescence waveforms for emission at 844.7 and 777.5 nm. The noise in these traces is due to the effect of the interpolating feature of the oscilloscope (see Section B) and the large fluctuations in the fluorescence signal between successive laser shots. Under all pressure conditions investigated, the emission at 844.7 nm from the initially excited ^3P level was much stronger. It should also be noted that the relative detection sensitivity (filter transmission plus photomultiplier sensitivity, the latter taken from manufacturer's specifications) was larger (4:1) for the collision-induced $^5\text{P} \rightarrow ^5\text{S}$ feature.

In addition to the differing intensities for the fluorescent decay of the initially excited $3P$ and collisionally populated $5P$ states, the two waveforms in Figure 3 have different temporal profiles. The waveform for the $3P$ state in Figure 3a is the usual exponential curve expected for the decay of an excited level, while that for the $5P$ state in Figure 3b builds up to the peak intensity after an induction period. The next section presents in detail the equations governing the time dependence of these emissions and shows how rate constants for the various kinetic processes can be extracted.

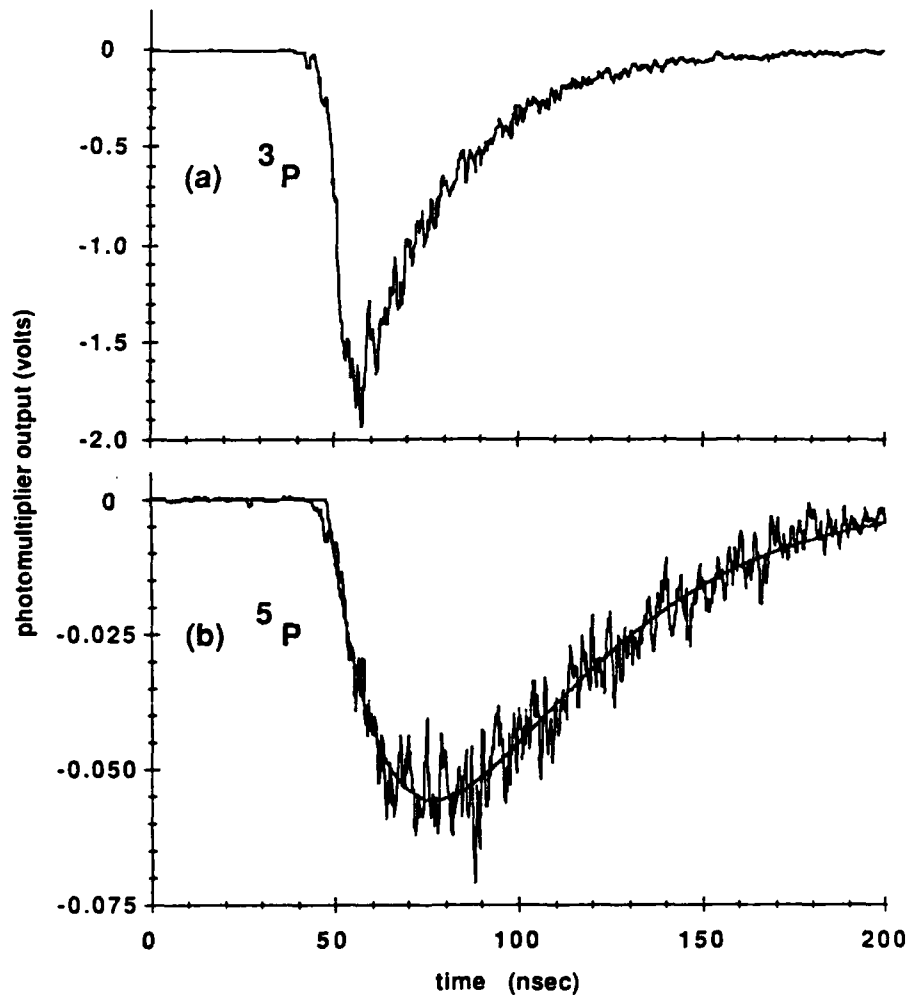


Figure 3. Waveforms for (a) the $3P \rightarrow 3S$ and (b) the $5P \rightarrow 5S$ Fluorescence Emission Upon Two-Photon Excitation of the $3p\ 3P$ State. Pressures: 1.47 Torr He and 0.30 Torr O_2 . These waveforms were acquired with the same photomultiplier voltage merely by channeling the detection filter.

B. Kinetic Equations:

The following equations govern the kinetics of decay and energy transfer of the $3p$ 3P and 5P electronic states of the oxygen atom:

$$dn_3/dt = -n_3k_3, \quad (1)$$

and

$$dn_5/dt = n_3k_{35} - n_5k_5, \quad (2)$$

where n_3 and n_5 are the concentrations of the 3P and 5P states, respectively, and k_3 and k_5 are the total removal rates by both radiative and collisional processes for the respective atomic states:

$$k_3 = k_3^r + k_3^Q(M)[M] \quad (3)$$

and

$$k_5 = k_5^r + k_5^Q(M)[M] . \quad (4)$$

Here the spontaneous decay rates are denoted by k_3^r and k_5^r , while the bimolecular quenching rate constants are indicated as $k_3^Q(M)$ and $k_5^Q(M)$. Equations (3) and (4) are written assuming there is only one quenching species, of concentration $[M]$, present. The generalization to several collision partners is obvious. These quenching rate constants represent the total rate of collisional removal of the relevant atomic species. The quantity k_{35} in Eq. (2) represents that portion of the collisional removal of the 3P state which results in energy transfer to the 5P state:



We write

$$k_{35} = k_{35}(M)[M] , \quad (6)$$

where $k_{35}(M)$ is the bimolecular rate constant for process.⁵

We assume that the two-photon laser excitation to the 3P state yields a concentration $n_3^{(0)}$ in this state at $t=0$. Equations (1) and (2) may be readily integrated. The 3P state follows a simple exponential decay:

$$n_3 = n_3^{(0)} \exp(-k_3t), \quad (7)$$

while the time dependence of the 5P state is given by the difference of two exponentials:

$$n_5 = \frac{n_3^{(0)} k_{35} [\exp(-k_5t) - \exp(-k_3t)]}{k_3 - k_5} \quad (8)$$

Thus, we see that the time dependence of the 3P population follows the usual exponential decay, while that of the 5P state builds up to a maximum after some delay.

Equation (7) shows that the 3P radiative lifetime and quenching rate constants may be determined by measurement of the decay lifetime $\tau = k_3^{-1}$ as a function of quench gas pressure, in the usual Stern-Vollmer treatment. The corresponding quantities for the 5P state must be determined in a nonlinear least squares treatment of the 5P concentration as a function of time, according to Eq. (8). The time dependence of the 3P and 5P concentrations can be determined from the emission intensities at 844.7 and 777.5 nm, respectively.

The $^3P \rightarrow ^5P$ transfer rate k_{35} cannot be determined from analysis of the fluorescence waveforms alone, but rather from the ratio of the integrated emission intensities. The integrated fluorescence intensity for the decay of the 3P state is proportional to

$$I_3 = k_3^F \int_0^\infty n_3 dt. \quad (9a)$$

With the help of Eq. (7), this equals

$$I_3 = n_3^{(0)} (k_3^F/k_3). \quad (9b)$$

The quantity in parentheses in Eq. (9b) may be identified with the fluorescence quantum yield for the 3P state. The integrated emission intensity for the 5P state is given by

$$I_5 = k_5^F \int_0^\infty n_5 dt, \quad (10a)$$

which, with Eq. (8), becomes

$$I_5 = k_{35} n_3^{(0)} k_5^F/k_5 k_3. \quad (10b)$$

Thus, the ratio of these integrated emission intensities equals

$$I_5/I_3 = (k_{35}/k_3) (k_5^F/k_5). \quad (11)$$

The rightmost quantity in parentheses in Eq. (11) is the 5P fluorescence quantum yield, while the ratio of k_{35}/k_3 represents the ratio of $^3P \rightarrow ^5P$ energy transfer collisions to 3P radiative decay events.

C. Quenching Rate Constants:

Quenching rate constants for the 3P state were determined from linear least squares fits of the logarithm of the $^3P \rightarrow ^3S$ emission as a function of time from fluorescence decay curves, similar to that presented in Figure 3a, at different quencher concentrations. A Stern-Vollmer plot for O_2 is presented in Figure 4a. In this figure, the abscissa is the total O_2 partial pressure including oxygen passing through the microwave discharge and added downstream. For measurement of both O_2 and N_2 quenching rate constants, helium and oxygen, at typical pressures of approximately 1.3 and 0.2 Torr, respectively, were passed through the discharge. Using the previously measured⁶ quenching rate constant for helium, we calculate that collisional removal by this species is small under our conditions, approximately $0.07 \times 10^7 \text{ s}^{-1}$. In principle, the transient free radical species generated by the discharge could also contribute to collisional quenching. However, we found

that the decay rate k_3 was the same with low (20 W) or high (50 W) microwave power applied to the cavity.

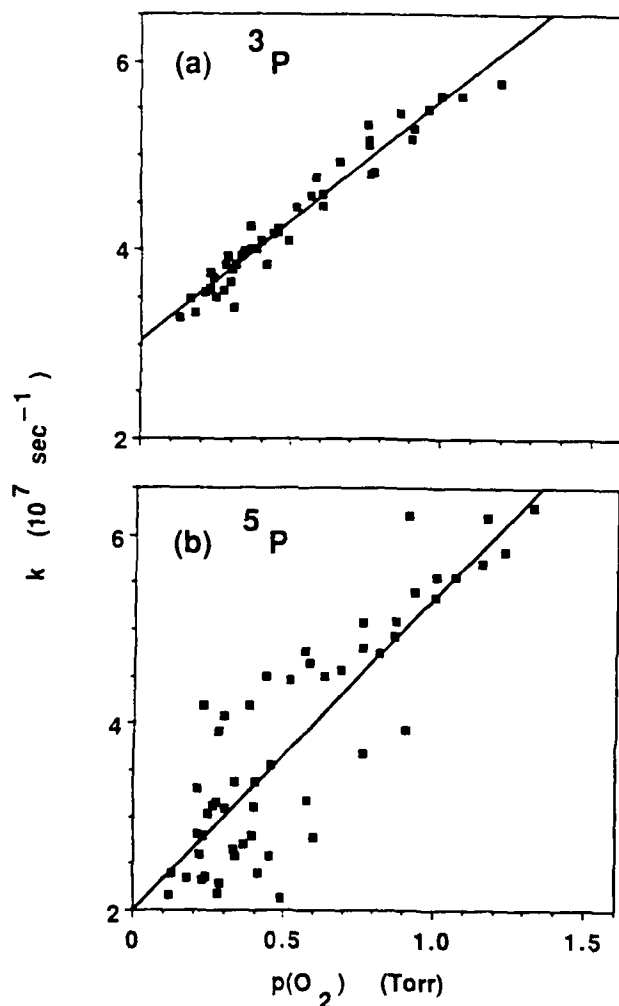


Figure 4. Stern-Volmer Plots for (a) the $^3\text{P} \rightarrow ^3\text{S}$ Emission at 844.7 nm and (b) the $^5\text{P} \rightarrow ^5\text{S}$ Emission at 777.5 nm as a Function of O_2 Quencher Partial Pressure

Linear least squares fits (the solid line in Figure 4a) of these data yields the following bimolecular rate constants listed in Table 1 for the total collisional removal rate of the ^3P state. The intercept for the O_2 plot yields a decay rate of $(3.05 \pm 0.15) \times 10^7 \text{ s}^{-1}$. Correcting for the expected contribution due to helium quenching (see above), we obtain the radiative decay rate for the ^3P state: $k_3^r = (2.98 \pm 0.15) \times 10^7 \text{ s}^{-1}$. This corresponds to an estimated ^3P radiative lifetime of $33.3 \pm 1.7 \text{ nsec}$. The quoted uncertainties for all rate constants represent 3 standard deviations.

Table 1. Bimolecular Rate Constants for Quenching and Collisional Transfer of the $3p\ ^3P$ and $5p$ States of the Oxygen Atom at Room Temperature

Collision Partner	Rate constant (molecule ⁻¹ cm ³ s ⁻¹)	This Study	Previous Determinations
O ₂	k ₃ ⁰	(7.8±0.8) X 10 ⁻¹⁰	(8.64±0.16) X 10 ⁻¹⁰ Ref. 8 (6.3±0.12) X 10 ⁻¹⁰ Ref. 6b
	k ₅ ⁰	(10.8±1.8) X 10 ⁻¹⁰	
	k ₃₅	6 X 10 ⁻¹¹ *	
N ₂	k ₃ ⁰	(5.87±0.15) X 10 ⁻¹⁰	(4.3±0.74) X 10 ⁻¹⁰ Ref. 6b (2.5±0.1) X 10 ⁻¹⁰ Ref. 1
	k ₃₅	2 X 10 ⁻¹¹ *	

*Estimated experimental uncertainty of a factor of 2.

The collisional and radiative decay rate for the $5p$ state was obtained from analysis of $5p + 5s$ decay curves such as that presented in Figure 3b. Because of the weakness of the $5p + 5s$ emission signals, this analysis was carried out only for O₂ quencher. The total decay rate k₅ was determined by nonlinear least squares fits¹⁸ using the expected functional form in Eq. (8) for the time dependence of the $5p$ population. In this fit, the decay rate k₃ for the $3p$ state was fixed at the value calculated from the Stern-Vollmer plot in Figure 4a for the O₂ partial pressure in the given scan. Parameters allowed to vary in this nonlinear fit were the decay rate k₅, an overall normalization constant (proportional to k₃₅), and the channel for which t=0. The solid line in Figure 3b represents the fit to the experimental data given in that plot.

The derived decay rates k₅ from nonlinear least squares analysis of $5p + 5s$ emission waveforms are presented in Figure 4b. It can be seen that the scatter of the calculated rate constants is large. This is due mainly to the smallness of these emission signals, which arise not directly from the initially populated state but rather by collisional transfer. A Stern-Vollmer analysis of these rate constants was performed (solid line in Figure 4b) and yield the following estimates for the bimolecular quenching rate constant by O₂ and the radiative decay rate: k₅⁰(O₂) = (10.8±1.8) X 10⁻¹⁰ molecule⁻¹ cm³ s⁻¹ (included in Table 1) and k₅^r = (2.01±0.35) X 10⁷ s⁻¹. This corresponds to an estimated radiative lifetime of 50±9 nsec.

D. Energy Transfer Rate Constants:

Equation (11) shows that measurement of the ratio of the integrated emission intensities for $5p + 5s$ and $3p + 3s$ fluorescence decay can yield the rate constant k₃₅ for collisional transfer from the $3p$ to the $5p$ state. Accordingly, a series of experiments were carried out to record these waveforms under identical pressure conditions. For a given partial pressure

of added quench gas, the fluorescence waveform for one of these radiative decay paths was recorded; then the filter was switched and the other recorded immediately thereafter. The integrated signals were calculated and their ratios corrected for the relative detection sensitivity at 844.7 and 777.5 nm.

Figure 5 displays the derived integrated $5p \rightarrow 5s$ to $3p \rightarrow 3s$ intensity ratios, corrected for the wavelength response of the photomultiplier, as a function of both added O_2 and added N_2 gas. The scatter in these data is again large, reflecting the large fluctuations in the fluorescence signal from laser shot to shot. Nevertheless, it can be seen that for both collision partners this ratio is always small and never increases beyond 5%.

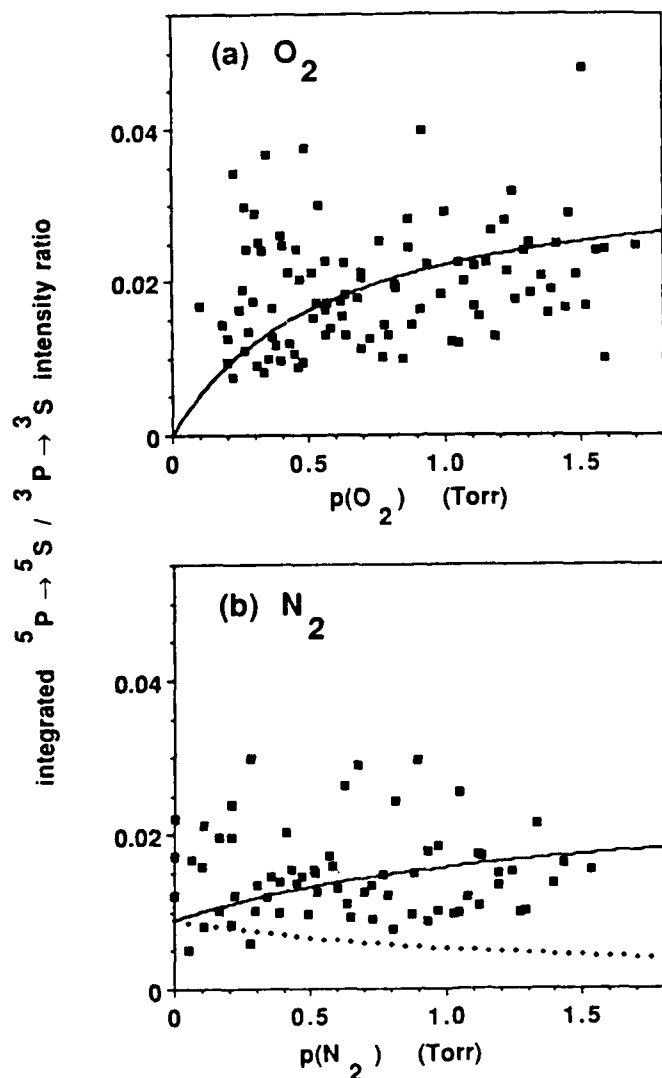


Figure 5. Ratio of the Integrated $5p \rightarrow 5s$ to $3p \rightarrow 3s$ Emission Intensity (Corrected for the Wavelength Sensitivity of the Photomultiplier) Versus Added (a) O_2 and (b) N_2 . The solid curves represent the best fits to the intensity ratio versus quench gas pressure. The dotted curve in (b) shows the expected intensity ratio if $k_{35}(N_2)$ were equal to zero.

In spite of the large experimental uncertainties in the integrated intensity ratio, we may still obtain estimates of the rate constants for $^3P \rightarrow ^5P$ collisional transfer. For the case of O_2 , for which the data are displayed in Figure 5a, the integrated intensity ratio can be expressed as a function of the O_2 density $n(O_2)$ as

$$\frac{I_5}{I_3} = \frac{A n(O_2)}{1+n(O_2)/n_0} \quad (12)$$

where

$$A = k_{35}(O_2)/k_3^r, \quad (13)$$

and

$$n_0 = k_5^r/k_5^0(O_2). \quad (14)$$

The quantity n_0 can be calculated from the Stern-Vollmer analysis (Figure 4(b)) for the 5P state and equals 1.9×10^{16} molecules cm^{-3} (or 0.58 Torr).

Thus, Eq. (12) can be fit to the data in Figure 5a by a linear least squares fit¹⁸ to determine the coefficient A in Eq. (12). Using our derived value for the 3P radiative decay rate k_3^r , we find that the rate constant $k_{35}(O_2)$ equals 6×10^{-11} molecule $^{-1}$ cm^3 s $^{-1}$. We estimate an uncertainty of approximately a factor of 2 in this value, due to the scatter in the determined intensity ratios given in Figure 5 and the uncertainty in the relative detection sensitivity. The contribution to the uncertainty in $k_{35}(O_2)$ due to possible error in k_3^r is less than that from the scatter in the measured intensity ratios. The solid curve in Figure 5a represents the best fit to the integrated intensity ratio as a function of added O_2 .

Because of the presence of a small amount of O_2 to generate oxygen atoms, the dependence of the integrated intensity ratio on added N_2 density $n(N_2)$ differs somewhat from Eq. (12). In this case, we have

$$\frac{I_5}{I_3} = \frac{B}{C+n(N_2)/n_N} + \frac{Dn(N_2)}{C+n(N_2)/n_N} \quad (15)$$

where

$$B = k_{35}(O_2) n(O_2)/k_3^r, \quad (16)$$

$$C = 1 + n(O_2)/n_0, \quad (17)$$

$$D = k_{35}(N_2)/k_3^r, \quad (18)$$

and

$$n_N = k_5^r/k_5^0(N_2). \quad (19)$$

The parameters B and C are known from the analysis of the O_2 data. We have not studied the quenching of the 5P state by N_2 . In view of the similarity of the 3P and 5P quenching rate constants by O_2 , within the large experimental uncertainties particularly of the latter, we assume that $k_{35}^O(N_2)$ in Eq. (19) equals the corresponding rate constant for the 3P state. We thus calculate n_N to equal 3.4×10^{16} molecules cm^{-3} (or 1.05 Torr).

The transfer rate constant $k_{35}(N_2)$ may be calculated by a linear least squares fit, similar to that used for the corresponding rate constant for O_2 , to determine the parameter D in Eq. (15). We find that $k_{35}(N_2)$ equals 2×10^{-11} molecule $^{-1}$ cm^3 s^{-1} , with an estimated factor of 2 uncertainty. The solid curve in Figure 5b represents the best fit to the integrated intensity ratio as a function of added N_2 . This value for $k_{35}(N_2)$ depends on assuming that the 3P and 5P quenching rate constants for N_2 are the same. If the 5P rate were only half as large, then the derived value for $k_{35}(N_2)$ would be reduced by ca. 30%, which is within the estimated experimental uncertainties. To show that $^3P \rightarrow ^5P$ collisional transfer is significant with N_2 collision partner, we have also plotted with a dotted curve in Figure 5b the expected integrated intensity ratio if $k_{35}(N_2)$ were equal to zero. The rate constants k_{35} for both O_2 and N_2 are also included in Table 1.

IV. DISCUSSION

Table 1 compares our quoted $3p\ ^3P$ total quenching rate constants with those determined in previous studies. Our value for O_2 agrees well with that of Bamford, et al.,⁸ and is somewhat higher than the most recent result^{6b} from Kohse-Hoinghaus and coworkers. The present result for the corresponding rate constant for quenching by N_2 is also slightly higher than that of Kohse-Hoinghaus and coworkers.^{6b} By contrast, the earliest measurement of the N_2 quenching rate constant by Bischel, et al.,¹ is considerably smaller than the present result and that of Ref. 6b. We do not know the reason for this discrepancy.

The present result for the $3p\ ^3P$ radiative lifetime (33.6 ± 1.7 nsec), derived from the intercept of the Stern-Vollmer plot for 3P quenching by O_2 (Figure 4a), agrees reasonably well with previous determinations of this lifetime. By similar observation of time-resolved two-photon laser-induced fluorescence, Bamford, et al.,⁸ Bittner, et al.,^{6b} and Kroll, et al.,¹⁹ obtain values of 34.7 ± 3.7 , 36.2 ± 0.69 , and 36 ± 4 nsec, respectively. The measurement of Bischel, et al.,¹ who also monitored the emission after two-photon laser excitation and report $\tau(3p\ ^3P) = 39.1 \pm 1.4$ nsec, and that of Bromander, et al.,²⁰ who employed a high frequency electron beam deflection technique and find $\tau(3p\ ^3P) = 40 \pm 3$ nsec, yield lifetimes somewhat longer than the more recent experimental results. There have been several earlier determinations, involving absolute emission intensity measurements, of the $3p\ ^3P \rightarrow 3s\ ^3S$ radiative decay rate, and hence $3p\ ^3P$ radiative lifetime, since the upper state has only one electric-dipole-allowed decay pathway. The compilation of Wiese, et al.,²¹ gives a value of $\tau(3p\ ^3P) = 35.7$ nsec. The theoretical calculations of Pradhan and Saraph²² yields a somewhat smaller result: $\tau(3p\ ^3P) = 30.3$ nsec. The former is in reasonable agreement with recent time-resolved experiments, while the latter appears to be slightly small.

Our experimental determination of the $3p\ ^5P$ radiative lifetime, $\tau(3p\ ^5P) = 50 \pm 9$ nsec, appears to be somewhat longer than previous estimates of this

quantity. The present measurement suffers from difficulties in extracting the 5P decay rate k_5 in a nonlinear least squares fit to $^5P \rightarrow ^5S$ emission waveforms with low signal to noise ratio such as that displayed in Figure 3b. There has been only one other time-resolved determination of the $3p\ ^5P$ radiative lifetime. Using the high-frequency electron beam deflection technique, Bromander, et al.,²⁰ report $\tau(3p\ ^5P) = 39 \pm 2$ nsec. The compilation of Wiese, et al.,²¹ yields a value of 29 nsec, while a result of 28 nsec is obtained from the calculations of Pradhan and Saraph.²² The oscillator strengths computed by Pradhan and Saraph²² have recently been shown by comparison with electron scattering results to be reliable to better than 20%, at least for transitions out of the ground $2p^4\ ^3P$ state.²³

To our knowledge, there have been no previous experimental determinations of collisional properties of the $3p\ ^5P$ state. While the exact value for the 5P quenching rate constant by O_2 may be uncertain because of difficulties such as those discussed in the previous paragraph, the present experiment nevertheless indicates that this quenching is large and comparable to that for the neighboring 3P state. In attempting to understand the variation of the rate constants for quenching of the nitrogen atom $3p\ ^4D$ state by the inert gases, Copeland, et al.,⁷ noted the importance of the availability of excited states in both the excited atom and the quencher to understand the mechanism of quenching. For the oxygen atom, it is interesting that the overall quenching rate for the $3p\ ^3P$ and 5P states by O_2 are both large, despite the fact that the former can be removed by excitation transfer to the 5P state, which lies only ca. 2000 cm^{-1} lower, while excitation transfer to lower O atom $3s$ states for the latter would require removal of ca. 12000 cm^{-1} (see Figure 1). This suggests that excited states of the O_2 collision partner may be of importance.

The ratio of the rate constants $k_{35}(M)$ to $k_3^0(M)$ equals the fraction f_T of 3P quenching collisions which result in excitation transfer to the lower-lying 5P state. Despite the factor of 2 uncertainty in our measured excitation transfer rate constants, it is nevertheless clear that $^3P \rightarrow ^5P$ collisional transfer explains only a small fraction of the 3P quenching. For O_2 and N_2 , we find that f_T equals approximately 8% and 3%, respectively. While f_T is significantly lower for the closed-shell N_2 molecule than for O_2 , nevertheless this excitation transfer process is not insignificant for the former. This suggests that the model for this process given in the Introduction may be too simplistic.

We surmise that the bulk of 3P quenching collisions occurs by excitation transfer to the collision partner, rather than collision-induced transitions to lower-lying oxygen atom states. This intermolecular excitation transfer would be expected to populate quencher electronic states whose energies lie close to that of the incident 3P state. The initial internal energy of the former is quite high, ca. 88600 cm^{-1} (see Figure 1), and both O_2 and N_2 possess a number of potential acceptor excited electronic states in this energy range.²⁴ As the initial excitation energy is greater than the O_2 and N_2 bond energies, dissociative excitation transfer can also occur.

The participation of excited acceptor states in the collisional decay of the 3P state would explain why the model for $^3P \rightarrow ^5P$ collision-induced transitions given in the Introduction is inadequate. Verification of the importance of intermolecular excitation transfer in the quenching of the $3p\ ^3P$

state could be obtained by observation of excited molecular emission, in the same way that we have shown the existence of intramolecular $3p \rightarrow 5p$ collisional transitions. For example, in the case of N_2 the well-known $C^3\Pi_u$ state has excitation energy very close to that of the O atom $3p$ state; this electronic state emits in the second positive system in the ultraviolet.²⁴ Quenching of the $3p$ state by N_2 can also proceed by a chemical path, namely $O(3p\ 3p) + N_2 \rightarrow NO + N$.

The large uncertainties in the rate constants $k_{35}(M)$ result from the large scatter in the measured integrated intensity ratios I_5/I_3 (see Figure 5). These fluctuations would be considerably reduced if the integrated signals I_5 and I_3 were measured simultaneously with two photomultiplier detectors, rather than sequentially as in the present experiment. In this way, the intensity ratio would be corrected for shot-to-shot fluctuations in the laser pulse energy and spectral profile. Unfortunately, modification of the apparatus to allow dual photomultiplier detection was not possible in this experimental study.

ACKNOWLEDGEMENT

We are indebted to Dr. Chen Hsu, of CRDEC at Edgewood, MD, for the loan of a frequency mixing crystal while our crystal was being repolished. BEF and AWM acknowledge partial support from the Air Force Office of Scientific Research, Directorate of Aerospace Sciences, Contract Number 88-0013. The work at Johns Hopkins University was supported in part by the National Science Foundation and the U.S. Army Research Office.

REFERENCES

1. W.K. Bischel, B.F. Perry, and D.R. Crosley, "Two-Photon Laser Induced Fluorescence in Oxygen and Nitrogen Atoms," Chem. Phys. Lett., Vol. 82, p. 85, 1981; "Detection of Fluorescence from O and N Atoms Induced by Two-Photon Absorption," Appl. Opt., Vol. 21, p. 1419, 1982.
2. R.P. Lucht, J.T. Salmon, G.B. King, D.W. Sweeney, and N.M. Laurendeau, "Two-Photon-Excited Fluorescence Measurement of Hydrogen Atoms in Flames," Opt. Lett., Vol. 8, p. 365, 1983.
3. M. Alden, H. Edner, P. Grafstrom, and S. Svanberg, "Two-Photon Excitation of Atomic Oxygen in a Flame," Opt. Commun., Vol. 42, p. 244, 1982.
4. M. Alden, A.L. Schawlow, S. Svanberg, W. Wendt, and P.L. Zhang, "Three-Photon-Excited Fluorescence Detection of Atomic Hydrogen in an Atmospheric Pressure Flame," Opt. Lett., Vol. 9, p. 211, 1984.
5. A.W. Miziolek and M.A. DeWilde, "Multiphoton Photochemical and Collisional Effects During Oxygen-Atom Flame Detection," Opt. Lett., Vol. 9, p. 390, 1984.
6. (a) U. Meier, K. Kohse-Hoinghaus, and Th. Just, "H and O Atom Detection for Combustion Applications: Study of Quenching and Laser Photolysis Effects," Chem. Phys. Lett., Vol. 126, p. 567, 1986; (b) J. Bittner, K. Kohse-Hoinghaus, U. Meier, and Th. Just, "Quenching of Two-Photon Excited H ($3s, 3d$) and O ($3p\ ^3P_{1,2,0}$) Atoms by Rare Gases and Small Molecules," Chem. Phys. Lett., Vol. 143, p. 571, 1988.
7. R.A. Copeland, J.B. Jeffries, A.P. Hickman, and D.R. Crosley, "Radiative Lifetime and Quenching of the $3p\ ^4D^0$ State of Atomic Nitrogen," J. Chem. Phys., Vol. 86, p. 4876, 1987.
8. D.J. Bamford, L.E. Jusinski, and W.K. Bischel, "Absolute Two-Photon Absorption and Three Photon Ionization Cross Sections for Atomic Oxygen Atoms," Phys. Rev. A, Vol. 34, p. 185, 1986.
9. J.E.M. Goldsmith, "Resonant Multiphoton Optogalvanic Detection of Atomic Hydrogen in Flames," Opt. Lett., Vol. 7, p. 437, 1982; "Resonant Multiphoton Optogalvanic Detection of Oxygen Atoms in Flames," J. Chem. Phys., Vol. 78, p. 1610, 1983.
10. J.E.M. Goldsmith, "Flame Studies of Atomic Hydrogen and Oxygen Using Resonant Multiphoton Optogalvanic Spectroscopy," 20th Symposium (International) on Combustion, The Combustion Institute, Pittsburgh, p. 13, 1984.
11. J.E.M. Goldsmith, "Photochemical Effects in Two-Photon Excited Fluorescence Detection of Atomic Oxygen in Flames," Appl. Optics, Vol. 26, p. 3566, 1987.
12. P.J.H. Tjossem and T.A. Cool, "Detection of Atomic Hydrogen in Flames by Resonance Two-Photon Ionization at 365 nm," Chem. Phys. Lett., Vol. 100, p. 479, 1983.

13. M. Alden, H.M. Hertz, S. Svanberg, and S. Wallin, "Imaging Laser-Induced Fluorescence of Oxygen Atoms in a Flame," Appl. Opt., Vol. 23, p. 325, 1984.
14. J.E.M. Goldsmith and R.J.M. Anderson, "Imaging of Atomic Hydrogen in Flames with Two-Step Saturated Fluorescence Detection," Appl. Opt., Vol. 24, p. 607, 1985.
15. C.E. Moore, Atomic Energy Levels, Vol. 1, NSRDS-NBS 35, US Government Printing Office, Washington, 1971.
16. M.H. Alexander, private communication.
17. D.W. Setser, ed., Reactive Intermediates in the Gas Phase, Academic, New York, 1979.
18. P.R. Bevington, Data Reduction and Error Analysis for the Physical Sciences, McGraw-Hill, New York, 1969.
19. S. Kroll, H. Lundberg, A. Persson, and S. Svanberg, "Time-Resolved Laser Spectroscopy of High-Lying States in Neutral Oxygen," Phys. Rev. Lett., Vol. 55, p. 284, 1985.
20. J. Bromander, N. Duric, P. Erman, and M. Larsson, "Lifetimes of Some Levels in Neutral Carbon, Nitrogen, and Oxygen," Phys. Scr., Vol. 17, p. 119, 1978.
21. W.L. Wiese, M.W. Smith, and B.M. Glennon, Atomic Transition Probabilities, Vol. 1, NSRDS-NBS 4, US Government Printing Office, Washington, 1966.
22. A.K. Pradhan and H.E. Saraph, "Oscillator Strengths for Dipole Transitions in Neutral Oxygen," J. Phys. B, Vol. 10, p. 3365, 1977.
23. J.P. Doering, E.E. Gulcicek, and S.O. Vaughan, "Electron Impact Measurement of Oscillator Strengths for Dipole-Allowed Transitions of Atomic Oxygen," J. Geophys. Res., Vol. 90, p. 5279, 1985.
24. K.P. Huber and G. Herzberg, Molecular Spectra and Molecular Structure. IV. Constants of Diatomic Molecules, Van Nostrand Reinhold, New York, 1979.

DISTRIBUTION LIST

<u>No. Of Copies</u>	<u>Organization</u>	<u>No. Of Copies</u>	<u>Organization</u>
12	Administrator Defense Technical Info Center ATTN: DTIC-DDA Cameron Station Alexandria, VA 22304-6145	1	Commander US Army Aviation Systems Command ATTN: AMSAV-DACL 4300 Goodfellow Blvd. St. Louis, MO 63120-1798
1	HQ DA (SARD-TR) Washington, DC 20310-0001	1	Director US Army Aviation Research and Technology Activity Ames Research Center Moffett Field, CA 94035-1099
1	Commander US Army Materiel Command ATTN: AMCDRA-ST 5001 Eisenhower Avenue Alexandria, VA 22333-0001	4	Commander US Army Research Office ATTN: R. Ghirardelli D. Mann R. Singleton R. Shaw P.O. Box 12211 Research Triangle Park, NC 27709-2211
1	Commander US Army Laboratory Command ATTN: AMSLC-DL Adelphi, MD 20783-1145		
1	Commander Armament RD&E Center US Army AMCCOM ATTN: SMCAR-MSI Picatinny Arsenal, NJ 07806-5000		
1	Commander Armament RD&E Center US Army AMCCOM ATTN: SMCAR-TDC Picatinny Arsenal, NJ 07806-5000	2	Commander Armament R&D Center US Army AMCCOM ATTN: SMCAR-LCA-G, D.S. Downs J.A. Lannon Dover, NJ 07801
1	Director Benet Weapons Laboratory Armament RD&E Center US Army AMCCOM ATTN: SMCAR-LCB-TL Watervliet, NY 12189-4050	1	Commander Armament R&D Center US Army AMCCOM ATTN: SMCAR-LC-G, L. Harris Dover, NJ 07801
1	Commander US Army Armament, Munitions and Chemical Command ATTN: SMCAR-ESP-L Rock Island, IL 61299-5000		

DISTRIBUTION LIST

<u>No. Of Copies</u>	<u>Organization</u>	<u>No. Of Copies</u>	<u>Organization</u>
1	Commander Armament R&D Center US Army AMCCOM ATTN: SMCAR-SCA-T, L. Stiefel Dover, NJ 07801	1	Commander Naval Air Systems Command ATTN: J. Ramnarace, AIR-54111C Washington, DC 20360
1	Commander US Army Missile Command ATTN: AMSMI-AS Redstone Arsenal, AL 35898-5000	1	Commander Naval Surface Weapons Center ATTN: J.L. East, Jr., G-23 Dahlgren, VA 22448-5000
2	Commander US Army Missile Command ATTN: AMSMI-RK, D.J. Ifshin W. Wharton Redstone Arsenal, AL 35898	2	Commander Naval Surface Weapons Center ATTN: R. Bernecker, R-13 G.B. Wilmot, R-16 Silver Spring, MD 20902-5000
1	Commander US Army Missile Command ATTN: AMSMI-RKA, A.R. Maykut Redstone Arsenal, AL 35898-5249	5	Commander Naval Research Laboratory ATTN: M.C. Lin J. McDonald F. Oran J. Shnur R.J. Doyle, Code 6110 Washington, DC 20375
1	Commander US Army Tank Automotive Cmd ATTN: AMSTA-TSL Warren, MI 48397-5000	1	Commanding Officer Naval Underwater Systems Center Weapons Dept. ATTN: R.S. Lazar/Code 36301 Newport, RI 02840
1	Director US Army TRADOC Analysis Cmd ATTN: ATAA-SL White Sands Missile Range, NM 88002-5502	1	Superintendent Naval Postgraduate School Dept. of Aeronautics ATTN: D.W. Netzer Monterey, CA 93940
1	Commandant US Army Infantry School ATTN: ATSH-CD-CSO-OR Fort Benning, GA 31905-5660	4	AFRPL/DY, Stop 24 ATTN: R. Corley R. Geisler J. Levine D. Weaver Edwards AFB, CA 93523-5000
1	Office of Naval Research Department of the Navy ATTN: R.S. Miller, Code 432 800 N. Quincy Street Arlington, VA 22217	1	AFRPL/MKPB, Stop 24 ATTN: B. Goshgarian Edwards AFB, CA 93523-5000

DISTRIBUTION LIST

<u>No. Of Copies</u>	<u>Organization</u>	<u>No. Of Copies</u>	<u>Organization</u>
1	AFOSR ATTN: J.M. Tishkoff Rolling Air Force Base Washington, DC 20332	1	Atlantic Research Corp. ATTN: M.K. King 5390 Cherokee Avenue Alexandria, VA 22314
1	AFWL/SUL Kirtland AFB, NM 87117-5800	1	Atlantic Research Corp. ATTN: R.H.W. Waesche 7511 Wellington Road Gainesville, VA 22065
1	Air Force Armament Laboratory ATTN: AFATL/DLODL Eglin AFB, FL 32542-5000	1	AVCO Everett Rsch. Lab. Div. ATTN: D. Stickler 2385 Revere Beach Parkway Everett, MA 02149
1	NASA Langley Research Center Langley Station ATTN: G.B. Northam/MS 168 Hampton, VA 23365	1	Battelle Memorial Institute Tactical Technology Center ATTN: J. Huggins 505 King Avenue Columbus, OH 43201
4	National Bureau of Standards ATTN: J. Hastie M. Jacox T. Kashiwagi H. Semerjian US Department of Commerce Washington, DC 20234	1	Cohen Professional Services ATTN: N.S. Cohen 141 Channing Street Redlands, CA 92373
1	OSD/SDIO/UST ATTN: L.H. Caveny Pentagon Washington, DC 20301-7100	1	Exxon Research & Eng. Co. ATTN: A. Dean Route 22E Annandale, NJ 08801
1	Aerojet Solid Propulsion Co. ATTN: P. Micheli Sacramento, CA 95813	1	Ford Aerospace and Communications Corp. DIVAD Division Div. Hq., Irvine ATTN: D. Williams Main Street & Ford Road Newport Beach, CA 92663
1	Applied Combustion Technology, Inc. ATTN: A.M. Varney P.O. Box 17885 Orlando, FL 32860	1	General Applied Science Laboratories, Inc. 77 Raynor Avenue Ronkonkama, NY 11779-6649
2	Applied Mechanics Reviews The American Society of Mechanical Engineers ATTN: R.E. White A.B. Wenzel 345 E. 47th Street New York, NY 10017	1	General Electric Armament & Electrical Systems ATTN: M.J. Bulman Lakeside Avenue Burlington, VT 05401

DISTRIBUTION LIST

<u>No. Of Copies</u>	<u>Organization</u>	<u>No. Of Copies</u>	<u>Organization</u>
1	General Electric Company 2352 Jade Lane Schenectady, NY 12309	2	Director Lawrence Livermore National Laboratory ATTN: C. Westbrook M. Costantino P.O. Box 808 Livermore, CA 94550
1	General Electric Ordnance Systems ATTN: J. Mandzy 100 Plastics Avenue Pittsfield, MA 01203	1	Lockheed Missiles & Space Co. ATTN: George Lo 3251 Hanover Street Dept. 52-35/B204/2 Palo Alto, CA 94304
2	General Motors Rsch Labs Physics Department ATTN: T. Sloan R. Teets Warren, MI 48090	1	Los Alamos National Lab ATTN: B. Nichols T7, MS-B284 P.O. Box 1663 Los Alamos, NM 87545
2	Hercules, Inc. Allegany Ballistics Lab. ATTN: R.R. Miller E.A. Yount P.O. Box 210 Cumberland, MD 21501	1	National Science Foundation ATTN: A.B. Harvey Washington, DC 20550
1	Honeywell, Inc. Government and Aerospace Products ATTN: D.E. Broden/ MS MN50-2000 600 2nd Street NE Hopkins, MN 55343	1	Olin Corporation Smokeless Powder Operations ATTN: V. McDonald P.O. Box 222 St. Marks, FL 32355
1	Honeywell, Inc. ATTN: R.E. Tompkins MN38-3300 10400 Yellow Circle Drive Minnetonka, MN 55343	1	Paul Gough Associates, Inc. ATTN: P.S. Gough 1048 South Street Portsmouth, NH 03801-5423
1	IBM Corporation ATTN: A.C. Tam Research Division 5600 Cottle Road San Jose, CA 95193	2	Princeton Combustion Research Laboratories, Inc. ATTN: M. Summerfield N.A. Messina 475 US Highway One Monmouth Junction, NJ 08852
1	IIT Research Institute ATTN: R.F. Remaly 10 West 35th Street Chicago, IL 60616	1	Hughes Aircraft Company ATTN: T.E. Ward 8433 Fallbrook Avenue Canoga Park, CA 91303

DISTRIBUTION LIST

<u>No. Of Copies</u>	<u>Organization</u>	<u>No. Of Copies</u>	<u>Organization</u>
1	Rockwell International Corp. Rocketdyne Division ATTN: J.E. Flanagan/HB02 6633 Canoga Avenue Canoga Park, CA 91304	3	Thiokol Corporation Wasatch Division ATTN: S.J. Bennett P.O. Box 524 Brigham City, UT 84302
4	Sandia National Laboratories Combustion Sciences Dept. ATTN: R. Cattolica S. Johnston P. Mattern D. Stephenson Livermore, CA 94550	1	United Technologies ATTN: A.C. Eckbreth East Hartford, CT 06108
1	Science Applications, Inc. ATTN: R.B. Edelman 23146 Cumorah Crest Woodland Hills, CA 91364	3	United Technologies Corp. Chemical Systems Division ATTN: R.S. Brown T.D. Myers (2 copies) P.O. Box 50015 San Jose, CA 95150-0015
1	Science Applications, Inc. ATTN: H.S. Pergament 1100 State Road, Bldg. N Princeton, NJ 08540	1	Universal Propulsion Company ATTN: H.J. McSpadden Black Canyon Stage 1 Box 1140 Phoenix, AZ 85029
3	SRI International ATTN: G. Smith D. Crosley D. Golden 333 Ravenswood Avenue Menlo Park, CA 94025	1	Veritay Technology, Inc. ATTN: E.B. Fisher 4845 Millersport Highway P.O. Box 305 East Amherst, NY 14051-0305
1	Stevens Institute of Tech. Davidson Laboratory ATTN: R. McAlevy, III Hoboken, NJ 07030	1	Brigham Young University Dept. of Chemical Engineering ATTN: M.W. Beckstead Provo, UT 84601
1	Thiokol Corporation Elkton Division ATTN: W.N. Brundige P.O. Box 241 Elkton, MD 21921	1	California Institute of Tech. Jet Propulsion Laboratory ATTN: MS 125/159 4800 Oak Grove Drive Pasadena, CA 91103
1	Thiokol Corporation Huntsville Division ATTN: R. Glick Huntsville, AL 35807	1	California Institute of Technology ATTN: F.E.C. Culick/ MC 301-46 204 Karman Lab. Pasadena, CA 91125

DISTRIBUTION LIST

<u>No. Of Copies</u>	<u>Organization</u>	<u>No. Of Copies</u>	<u>Organization</u>
1	University of California, Berkeley Mechanical Engineering Dept. ATTN: J. Daily Berkeley, CA 94720	3	Georgia Institute of Technology School of Aerospace Engineering ATTN: E. Price W.C. Strahle B.T. Zinn Atlanta, GA 30332
1	University of California Los Alamos Scientific Lab. P.O. Box 1663, Mail Stop B216 Los Alamos, NM 87545	1	University of Illinois Dept. of Mech. Eng. ATTN: H. Krier 144MEB, 1206 W. Green St. Urbana, IL 61801
2	University of California, Santa Barbara Quantum Institute ATTN: K. Schofield M. Steinberg Santa Barbara, CA 93106	1	Johns Hopkins University/APL Chemical Propulsion Information Agency ATTN: T.W. Christian Johns Hopkins Road Laurel, MD 20707
2	University of Southern California Dept. of Chemistry ATTN: S. Benson C. Wittig Los Angeles, CA 90007	1	University of Michigan Gas Dynamics Lab Aerospace Engineering Bldg. ATTN: G.M. Faeth Ann Arbor, MI 48109-2140
1	Case Western Reserve Univ. Div. of Aerospace Sciences ATTN: J. Tien Cleveland, OH 44135	1	University of Minnesota Dept. of Mechanical Engineering ATTN: E. Fletcher Minneapolis, MN 55455
1	Cornell University Department of Chemistry ATTN: T.A. Cool Baker Laboratory Ithaca, NY 14853	3	Pennsylvania State University Applied Research Laboratory ATTN: K.K. Kuo H. Palmer M. Micci University Park, PA 16802
1	Univ. of Dayton Rsch Inst. ATTN: D. Campbell AFRPL/PAP Stop 24 Edwards AFB, CA 93523	1	Pennsylvania State University Dept. of Mechanical Engineering ATTN: V. Yang University Park, PA 16802
1	University of Florida Dept. of Chemistry ATTN: J. Winefordner Gainesville, FL 32611		

DISTRIBUTION LIST

<u>No. Of Copies</u>	<u>Organization</u>	<u>No. Of Copies</u>	<u>Organization</u>
1	Polytechnic Institute of NY Graduate Center ATTN: S. Lederman Route 110 Farmingdale, NY 11735	1	University of Texas Dept. of Chemistry ATTN: W. Gardiner Austin, TX 78712
2	Princeton University Forrestal Campus Library ATTN: K. Brezinsky I. Glassman P.O. Box 710 Princeton, NJ 08540	1	University of Utah Dept. of Chemical Engineering ATTN: G. Flandro Salt Lake City, UT 84112
1	Princeton University MAE Dept. ATTN: F.A. Williams Princeton, NJ 08544	1	Virginia Polytechnic Institute and State University ATTN: J.A. Schetz Blacksburg, VA 24061
1	Purdue University School of Aeronautics and Astronautics ATTN: J.R. Osborn Grissom Hall West Lafayette, IN 47906	1	Commandant USAFAS ATTN: ATSF-TSM-CN Fort Sill, OK 73503-5600
1	Purdue University Department of Chemistry ATTN: E. Grant West Lafayette, IN 47906	1	F.J. Seiler Research Lab (AFSC) ATTN: S.A. Shakelford USAF Academy, CO 80840-6528
2	Purdue University School of Mechanical Engineering ATTN: N.M. Laurendeau S.N.B. Murthy TSPC Chaffee Hall West Lafayette, IN 47906	1	Freedman Associates ATTN: E. Freedman 2411 Diana Road Baltimore, MD 21209-1525
1	Rensselaer Polytechnic Inst. Dept. of Chemical Engineering ATTN: A. Fontijn Troy, NY 12181		<u>Aberdeen Proving Ground</u> Dir, USAMSAA ATTN: AMXSY-D AMXSY-MP, H. Cohen Cdr, USATECOM ATTN: AMSTE-TO-F Cdr, CRDEC, AMCCOM ATTN: SMCCR-RSP-A SMCCR-MU SMCCR-SPS-IL
1	Stanford University Dept. of Mechanical Engineering ATTN: R. Hanson Stanford, CA 94305		

USER EVALUATION SHEET/CHANGE OF ADDRESS

This laboratory undertakes a continuing effort to improve the quality of the reports it publishes. Your comments/answers below will aid us in our efforts.

- 1. Does this report satisfy a need? (Comment on purpose, related project, or other area of interest for which the report will be used.) _____
- 2. How, specifically, is the report being used? (Information source, design data, procedure, source of ideas, etc.) _____
- 3. Has the information in this report led to any quantitative savings as far as man-hours or dollars saved, operating costs avoided, or efficiencies achieved, etc? If so, please elaborate. _____
- 4. General Comments. What do you think should be changed to improve future reports? (Indicate changes to organization, technical content, format, etc.) _____

BRL Report Number _____ Division Symbol _____

Check here if desire to be removed from distribution list. _____

Check here for address change. _____

Current address: Organization _____
Address _____

-----FOLD AND TAPE CLOSED-----

Director
U.S. Army Ballistic Research Laboratory
ATTN: SLCBR-DD-T (NEI)
Aberdeen Proving Ground, MD 21005-5066

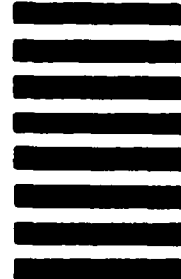
OFFICIAL BUSINESS
PENALTY FOR PRIVATE USE \$300



NO POSTAGE
NECESSARY
IF MAILED
IN THE
UNITED STATES

BUSINESS REPLY LABEL
FIRST CLASS PERMIT NO. 12062 WASHINGTON D. C.

POSTAGE WILL BE PAID BY DEPARTMENT OF THE ARMY



Director
U.S. Army Ballistic Research Laboratory
ATTN: SLCBR-DD-T (NEI)
Aberdeen Proving Ground, MD 21005-9989